Receptor binding and escape from Beta antibody responses drive Omicron-B.1.1.529 evolution

Jiří Zahradník[1,#], Aekkachai Tuekprakhon[2,#], Helen M. Ginn[3,#], Helen M.E. Duyvesteyn[4], Mohammad Bahar[4], Suman Khan[1], Ori Avinoam[1], Daming Zhou[4,5], Rungtiwa Nutalai[2], Piyada Supasa[2], Beibei Wang[2,5], Wanwisa Dejnirattisai[2], Chang Liu[2], Aiste Dijokaite[2], Nigel Temperton[6], Juthathip Mongkolsapaya[2,7] ,Elizabeth E. Fry[4], Ren Jingshan[4,*], Gavin R. Screaton[2,5,*], Gideon Schreiber[1,*], David I. Stuart[1,3,8*,^]

1. Department of Biomolecular Sciences, Weizmann Institute of Science, Rehovot, Israel
2. Wellcome Centre for Human Genetics, Nuffield Department of Medicine, University of Oxford, Oxford, UK
3. Diamond Light Source Ltd, Harwell Science & Innovation Campus, Didcot, UK
4. Division of Structural Biology, Nuffield Department of Medicine, University of Oxford, The Wellcome Centre for Human Genetics, Oxford, UK
5. Chinese Academy of Medical Science (CAMS) Oxford Institute (COI), University of Oxford, Oxford, UK
6. Viral Pseudotype Unit, Medway School of Pharmacy, University of Kent and Greenwich, Chatham Maritime, Kent ME4 4TB, UK
7. Siriraj Center of Research Excellence in Dengue & Emerging Pathogens, Dean Office for Research, Faculty of Medicine Siriraj Hospital, Mahidol University, Thailand.
8. Instruct-ERIC, Oxford House, Parkway Court, John Smith Drive, Oxford, UK

# These authors contributed equally to this work.

* corresponding authors: ren@strubi.ox.ac.uk, dave@strubi.ox.ac.uk, gavin.screaton@medsci.ox.ac.uk, gideon.schreiber@weizmann.ac.il

^ Lead contact

Summary

On the 24th November 2021 the sequence of a new SARS CoV-2 viral isolate spreading rapidly in Southern Africa was announced. Omicron contains a total of 30 substitutions plus deletions and an insertion in Spike, far more than any previously reported variant. The mutations include those previously identified by *In-vitro* evolution to contribute to high-affinity binding to ACE2, including mutations Q498R and N501Y critical in forming additional interactions in the interface. Together with increased charge complementarity between the RBD and ACE2, these substantially increase affinity and potentially virus transmissibility through increased syncytia formation. Further mutations promote immune evasion. We have studied the binding of a large panel of potent monoclonal antibodies generated from early pandemic or Beta infected cases. Mutations in Omicron will likely compromise the binding of many of these and additionally, the binding of antibodies under commercial development, however residual binding should provide protection from severe disease.

Introduction

Since the end of 2020 a series of viral variants have emerged in different regions where some have caused large regional outbreaks, Alpha (Supasa et al., 2021) and more recently Delta (Liu et al., 2021a) have had the greatest reach, whilst Beta (Zhou et al., 2021), Gamma (Dejnirattisai et al., 2021b) and Lambda (Colmenares-Mejia et al., 2021) although causing large outbreaks in Southern Africa and South America respectively, did not become dominant forms in other parts of the World. Beta caused a massive outbreak in South Africa, although latterly it has been displaced by Delta. The increased infectivity of these strains was attributed to two factors, one was increased binding affinity to the ACE2 receptor and the second was immune evasion. A relation between higher binding affinity of the receptor binding domain

(RBD) of the spike protein and higher infectivity has been previously suggested (Starr et al., 2020; Zahradnik et al., 2021b). Indeed, mutations in the RBD of Alpha, Beta, Gamma and Delta variants are associated with an increased affinity towards ACE2, by 3.5, 6, 12.5 and 1.5-fold, or 7, 19, 19 and 2-fold respectively measured in independent laboratories (Dejnirattisai et al., 2021a; Liu et al., 2021a; Supasa et al., 2021; Zahradnik et al., 2021b; Zhou et al., 2021). Interestingly, yeast surface displayed selection of randomly mutated RBD selected for tighter ACE2 binding selected the mutations present in the variants of concern N501Y (Alpha, Beta, Gamma) and E484K (Beta, Gamma), variants of interest F490S (Lambda) or multiple other variants, for instance S477N (Zahradnik et al., 2021b). In addition, the mutation Q498R was selected, and shown to have a major contribution to binding (in epistasis with N501Y), raising the concern that a new variant that includes the different affinity enhancing mutations may arise (Zahradnik et al., 2021b).

The rapid emergence of Omicron (https:www.who.int/news/item/26-11-2021-classification-of-omicron-(bi1.1.529)-sars-cov-2-variant-of-concern) on the background of high Beta immunity implies that the virus may have evolved to escape neutralization by Beta specific serum (Liu et al., 2021b). Within spike (S), Omicron has 30 substitutions, deletion of 6 residues and insertion of 3 residues, whilst in all the other proteins there are a total of 16 substitutions and 7 residue deletions. Particular hotspots for the mutations are the ACE2 receptor binding domain (RBD) (15 amino acid substitutions) and the N-terminal domain (NTD) (3 deletions, 1 insertion, 4 substitutions). In-depth studies by a large number of laboratories have shown the RBD and NTD as the site of binding of the most potent monoclonal antibodies (mAbs) (Cerutti et al., 2021; Dejnirattisai et al., 2021a; Rapp et al., 2021; Zost et al., 2020) and the RBD is the

site of binding of various mAbs in clinical development (Baum et al., 2020; Dong et al., 2021; Pinto et al., 2020; Starr et al., 2021).

S mediates cellular interactions. It is a dynamic, trimeric structure (Walls et al., 2020; Walls et al., 2017) which can be lipid bound (Toelzer et al., 2020) and tightly associated in a 'closed' form or unfurled to expose one or more RBDs allowing both receptor binding and increased access to neutralising antibodies. Once bound to a cell, S undergoes cleavage and a drastic elongation converting it to the post fusion form. Most potent neutralizing antibodies target the ACE2 footprint (Dejnirattisai et al., 2021a; Lan et al., 2020; Liu et al., 2021b) occupying ~880 A^2 at the outermost tip of the RBD (the neck and shoulders referring to the torso analogy (Dejnirattisai et al., 2021a)), preventing cell attachment. A proportion of antibodies are able to cross-neutralize different variants (Liu et al., 2021b) and a few of these bind to a motif surrounding the N-linked glycan at residue 343 (Dejnirattisai et al., 2021a; Liu et al., 2021b). These antibodies, exemplified by S309 (Pinto et al., 2020) can cross-react with SARS-CoV-1 but do not block ACE2 interaction and their mechanism of action may be to destabilize the S-trimer. Neutralizing anti-NTD mAbs do not block ACE2 interaction and bind to a so-called supersite on the NTD (Cerutti et al., 2021; Chi et al., 2020), however they generally fail to give broad protection as the supersite is disrupted by a variety of NTD mutations present in the variants of concern. Moreover, some NTD domain binding antibodies were shown to have an infectivity-enhancing effect by induction of S open state (Liu et al., 2021c).

In this report we investigate the different factors contributing to the high mutation load and potential high infectivity of Omicron. For example, mutations in non-structural proteins (NSPs) may impact polymerase fidelity (Moeller et al., 2021), perhaps explaining the extreme

mutational cargo. Mutations in the MPro protease (Owen et al., 2021), papain-like protease (Gao et al., 2021) or polymerase (Gao et al., 2020) may escape small molecule inhibition. Utilizing a large bank of structures (n=29) from panels of potent monoclonal antibodies generated following infection with early pandemic Wuhan related strains (Dejnirattisai et al., 2021a) (n=13) together with a new set of structures (n=16) of potent mAbs generated from individuals infected with Beta, many of which bind to the three mutated residues in Beta RBD (K417N, E484K, N501Y) (Liu et al., 2021b), we have modelled their potential to neutralize Omicron. The numerous mutations present in Omicron RBD, which we propose to have been generated to escape the antibody response, quite likely Beta, are predicted to compromise or knock out binding of the vast majority of potent monoclonal antibodies, including most if not all mAb for prophylactic or clinical use (Baum et al., 2020). A second source for higher infectivity is the cluster of mutations in the RBD, also selected by *in vitro* evolution for tighter ACE2 binding (Zahradnik et al., 2021a; Zahradnik et al., 2021b) which include 7 of the Omicron RBD mutations. In particular Q498R, not found in previous lineages, was shown to confer high affinity binding (epistatic with N501Y) (Zahradnik et al., 2021a; Zahradnik et al., 2021b). It is suggested that the presence of Q498R acts as a pivot point on ACE2 enabling the virus to mutate other residues within the receptor footprint without compromising cell attachment but enabling immune evasion. We speculate about further changes that may allow the mutation at residue 498 to be tolerated.

Results

Phylogeny of Omicron

On average, a mutation is inserted into the genome of SARS-CoV-2 every second infection. Such mutations generate intra-host diversity upon which selection then acts, with the viral

load being a critical parameter (Valesano et al., 2021). As a result, the virus is constantly changing. The median number of sequences that harbor a mutation at any given position is 570 (out of 4.7 million genomic sequences in GISAID; Nov 14, 2021), however rather few of these are enriched, with less than 10% of amino-acids having over 10,000 sequenced mutations. Enrichment of a mutation at a given position suggests increased virus fitness endowing a selective advantage (Martin et al., 2021; Zahradnik et al., 2021c). If a specific mutation arises independently in different lineages, it implies an even greater advantage in fitness. Omicron has changes throughout its proteome but S changes dominate, with 30 amino acid substitutions plus 6 residues deleted and 3 inserted (**Figure 1 and 2**). Ten of these were found previously in at least two lineages (D614G was mutated early on and maintained throughout). Of those ten, six have the same amino-acid substitution in >75% of the sequences, and only one (E484A) has a unique substitution in Omicron (in Beta and Gamma it is a Lys). **Figure 1B** shows the number of mutant sequences per residue at positions undergoing mutations in independent lineages. This can be interpreted in two ways, one is that the later mutations are epistatic to one another and thus are more difficult to reach, or that they do not contribute to virus fitness.

The Omicron RBD has 1/1, 2/3, 1/3 and 1/2 changes in common with the RBDs of Alpha, Beta, Gamma and Delta variants respectively (**Figure 2B-F**). Since there are 15 changes in total in the RBD, this gives few clues to the origins of the variant. The NTD also has numerous changes, including 4 amino acid substitutions, 6 amino acids deleted and 3 amino acids inserted. Of these 3/3 Alpha deletions are in common with Omicron, Delta has 1/3 substitutions in common whilst there are no changes in common with Beta or Gamma. In particular several of these mutations occur in residues conserved in SARS-CoV-1 and many other Sarbecoviruses

(**Figure 1**). These observations agree with the Pango classification (Rambaut et al., 2020) which places Omicron at a substantial distance from all other variants, with the simplest explanation for its evolution being that it is derived by extensive, likely long-term evolution from a relatively early virus. It is less likely to have evolved in a single immunocompromised individual, as this would not explain the extreme accumulation of ACE2 affinity enhancing mutations, which were not observed in these cases (Borges et al., 2021). Thus, it is more likely to have evolved in rural, unmonitored populations. What is clear from the ratio of nonsynonymous to synonymous mutations (only one synonymous mutation in all of S) is that the evolution has been driven by strong selective pressure on S.

Although S has the largest concentration of changes, there are mutations in many non-structural proteins. Nsp12 Polymerase (PDB:7B3B) (Gao et al., 2020) bears a single mutation in Omicron, P323L, distant from the active site targeted by compounds in use or in clinical trials, whilst the Nsp14 N-terminal exonuclease domain (PDB:7N0D) (Moeller et al., 2021) important in proofreading, again has a single mutation, I42V, distal to the active site. These observations suggest that the large number of mutations in Omicron is not being driven by reduced polymerase fidelity. Nsp5 Mpro protease (PDB:7RFW) (Owen et al., 2021) has a single mutation, P132H, distal to the active site targeted by the Pfizer PF-07321332 compound and Nsp3 has no mutations close to either the active site of the papain-like protease (Gao et al., 2021) or the macro domain inhibitor site. Whilst allosteric effects cannot be completely ruled out, there is little apparent significance to these changes which probably would not impact on small molecule therapeutics currently in use or development. This may reflect the lack of selective pressure to date on these proteins.

Mapping of Omicron RBD mutations compared to Alpha, Beta, Gamma and Delta

The Alpha variant has a single change in the RBD at N501Y (**Figure 2D**) (Supasa et al., 2021) which occupies the right shoulder and contributes to the ACE2 binding footprint. Beta has two further mutations in the RBD: K417N and E484K, at back of the neck and left shoulder respectively (**Figure 2E**), also part of the ACE2 footprint (**Figure 2C**) (Zhou et al., 2021). Gamma mutations are similar: K417T, E484K, N501Y (Dejnirattisai et al., 2021b). Delta mutations, L452R front of neck, T478K far side of left shoulder, fall just peripheral to the ACE2 binding footprint (**Figure 2F**) (Liu et al., 2021a). Of the 15 Omicron changes in the RBD, nine map to the ACE2 binding footprint: K417N, G446S, S477N, E484A, Q493R, G496S, Q498R, N501Y, Y505H with N440K and T478K just peripheral (**Figure 2B-C**). Aside from these, mutations occur on the right flank: G339D, S371L, S373P and S375F (**Figure 2B**), the last three of which are adjacent to a lipid binding pocket (**Figure 3A**) (Toelzer et al., 2020). This pocket has been seen occupied by a lipid similar to linoleic acid in an unusually rigid state of S where all RBDs are found in a locked-down configuration stabilised by lipid-bridged quaternary interactions between adjacent RBDs. However, this lipid bound form has been rarely seen, instead the pocket is usually empty and collapsed, with the RBD alternating between looser down and up conformations. We presume that this is because the pocket readily empties of lipid during protein purification, indeed rapidly prepared virus particles tend to have the RBDs closer to the locked down state. Loss of lipid would thereby promote RBD presentation to the target cell.

In order to gain insight into the possible structural impact of the numerous RBD mutations we used Alphafold2 (Jumper et al., 2021) to predict the Omicron RBD structure (**Figure 3A and Figure S1**). Overlaying the 5 top ranked solutions, all were very similar to each other and

to the early pandemic reference structure (for residues 334 to 528 the RMSD for the 195 Ca atoms was 0.71 Å between the top ranked Alphafold2 prediction and the early pandemic structure). There was only one region of significant, but still relatively minor, difference in the region of the triple serine mutation 371-375 (numbering for the early pandemic virus), on the right flank (**Figure 3A**). These mutations S371L, S373P, S375F all change from small flexible polar serine residues to bulkier, less flexible hydrophobic residues. Interestingly, all the Omicron S mutations involve single codon changes apart from S371L which requires two changes from TCC to CTC indicative of an underlying strong selection pressure and biological function to this change. The structure is not markedly altered, however, it is exactly this region of the structure that undergoes a large conformation change when lipid is bound into the pocket. The serine rich loop opens, allowing the attached helix to swing out and open the pocket for lipid binding. We suggest that increased rigidity and the entropic penalty of exposing hydrophobic residues will disfavour lipid binding to Omicron. We suggest that this will have an effect on the properties of the virus, explaining the selection of this apparently concerted series of changes. The most likely effect would be to increase the propensity for RBD-up states, as has been observed for other variants (Gobeil et al., 2021), especially in the early stages of release from the cell.

Omicron NTD mutations

The mutations seen in the NTD lie on exposed flexible loops, which differ from those in SARS-CoV-1 and are likely to be antigenic (**Figure 3B**). In summary, the pattern of deletions and insertions seen in Omicron consistently moves those loops that are most different from SARS-CoV-1 to being more SARS-CoV-1-like, at least in length. In line with this, Alphafold2 predictions (**Figure 3C**) of the Omicron NTD place it intermediate between the Wuhan SARS-

CoV-2 NTD and SARS-CoV-1 NTD (RMSD between top ranked Alphafold2 model and SARS-CoV-2 0.7 Å for 222 residues, compared to 0.9 Å for 211 residues for SARS-CoV-1), the latter having generally shorter surface loops, in-line with deletions in Omicron. Deletions have been observed in other SARS-CoV-2 variants but with no particular pattern. Of the N1, N3 and N5 loops which comprise the antibody supersite, Omicron has a substitution at G142D and deletion of residues 143-145 in N3 which would mitigate against binding by a number of potent neutralizing antibodies e.g. 4A8 and 159 (Chi et al., 2020; Dejnirattisai et al., 2021b) (**Figure 3B**). The deletion of residues 69 and 70 in N2 has also occurred in the Alpha variant whilst the deletion at residue 211, substitution at 212 and insertion at 214 are unique to Omicron. All these changes are on the outer surface and likely antigenic (**Figure 3B**).

Effect on RBD/ACE2 Interaction

Fitness of a virus can stem from its higher infectivity or from evasion of the immune system. One way to identify mutations that increase binding affinity is by selection using a randomly mutated RBD displayed on the yeast surface for ACE2 binding. Mutations fixed for higher affinity binding included N501Y, E484K, S477N and most prominently, Q498R (Iota) (**Figure 4A**) (Zahradnik et al., 2021b). Interestingly, Q498R was selected only at later stages. This is explained by the 2-fold reduction in affinity as a single mutation (**Figure 4A**). However, in combination with the N501Y mutation, the affinity is increased 26-fold, more than any other mutation analyzed. Adding to this the S477N mutation, one obtains a 37-fold increase in binding (**Figure 4B**). These three mutations, selected through in vitro evolution, were found together, for the first time in the Omicron variant. In the light of the in vitro selection data the mutation of E484 to Ala, instead of the Lys found in Beta and Gamma variants is surprising, the reason for this will be discussed later. However, the effect of E484A versus E484K on

binding (as calculated from deep mutational scanning (Starr et al., 2020)) seems to be small (**Figure 4A, 4B**). While K417N (found in the Beta variant) on its own decreases binding, in combination with other mutations it seems to be neutral. Another mutation neutral for binding is T478K, which has been reported to affect binding of neutralizing antibodies in Delta (Liu et al., 2021a; Liu et al., 2021b; Mlcochova et al., 2021). The combination of mutations S477N, E484K, Q498R and N501Y was the most dominant in the yeast display, reaching fixation. Following repeated rounds of selection, RBD-62 (I358F, V445K, N460K, I468T, T470M, S477N, E484K, Q498R, N501Y) emerged as the highest affinity clone with a 1000-fold increase in affinity for ACE2 from 17 nM for Wuhan RBD to 16 pM for RBD-62. It is striking that the key contributors for the high affinity of RBD-62 are present in Omicron. Interestingly, the combination of mutations K417M, E484K, Q493R, Q498R and N501Y also emerged after 30 passages in mouse lungs (Wong et al., 2021). This mouse-adapted virus was highly virulent and caused a more severe disease. The appearance of E484K, Q493H/R, Q498R and N501Y in yeast display and mouse adaptation experiments is a strong indication that immune pressure is not required for their selection, but rather, tighter binding to ACE2, likely facilitating more efficient transmission.

The Omicron mutations S477N, E484A, Q498R and N501Y are similar to those in RBD-62 making it the closest known structure and therefore we use this structure for analysis. The mode of binding of the Omicron/RBD-62 mutations to ACE2 is shown in detail in **Figure 4C (inset boxes), 4D and 4E**. Mutations in Omicron RBD, which might be expected to contribute rather little to binding are S373P, S375F, K417N, N440K, T478K, Q493R and Y505H, however several of these contribute to a more positive charged RBD surface, which will assist binding by complementing the negatively charged surface of ACE2 in its S binding site (**Figure 4F**).

Additional mutations to positive charged residues also emerged in RBD-62 (V445K, N460K), resulting in a much faster rate of association for ACE2 (Zahradnik et al., 2021b).

Increased ACE2 affinity may enhance syncytia formation

Enhanced fusogenicity and syncytia formation has been described for Alpha and Beta infection and is most pronounced for delta where it was linked to acquisition of the P681R (leading to enhanced furin cleavage) and the D614G mutations (Mlcochova et al., 2021; Saito et al., 2021). This indicates that optimization of the furin binding site contributes to faster cleavage and more syncytia formation. Increased syncytia formation with the D614G mutation may be associated with changes in S flexibility (Plante et al., 2021), but the exact mechanism is unknown. To determine whether increased RBD/ACE2 binding affinity can play a role in syncytia formation we used the RBD-62 S chimera and performed detailed syncytia formation analysis (**Figure 5**). Unexpectedly, the RBD-62 S chimera dramatically promotes syncytia formation, particularly the formation of larger conglomerates, an effect enhanced by the addition of D614G. Based on the similarity between RBD-62 and Omicron-RBD and the presence of two key mutations in the furin cleavage area, H655Y and P681H (Escalera et al., 2021), we speculate that S protein from the Omicron variant is highly fusogenic.

Extreme RBD/ACE2 affinity does not limit neutralization

The extreme affinity of RBD-62 for ACE2 is higher than most antibody affinities and we wondered whether this would compromise the neutralization of viruses expressing RBD-62 (**Figure S2**). For biosafety reasons we chose not to express RBD-62 in an infectious SARS-CoV-2 virus and instead expressed an RBD-62 chimera with Wuhan spike in a lentiviral pseudovirus

system. RBD-62 pseudotyped virus remained infectious. We next tested neutralization of RBD-62 with a panel of potent monoclonal antibodies we have previously reported to SARS-CoV-2 (Dejnirattisai et al., 2021a). As expected a number of antibodies were vulnerable to the mutations present in RBD-62, however those antibodies that we know from structural analysis bind to epitopes that are not mutated in RBD-62 such as mAb 40, 88, 222 and 253 (which are ACE2 blockers) showed no reduction in neutralization of RBD-62. These results indicate that extreme affinity of RBD for ACE2 does not reduce antibody neutralization presumably because the antibodies bind before ACE2 engagement and have a sufficiently long off rate to prevent engagement with ACE2.

Effect of Omicron mutations on Wuhan antibody responses

Our panel of neutralizing antibodies isolated from cases infected with early pandemic viruses (Wuhan) were mapped together with other published structures to 5 epitopes (based on the position of the centre of gravity of each antibody) either by direct structural studies or competition analyses (Dejnirattisai et al., 2021a). According to the torso analogy (Dejnirattisai et al., 2021a) these were designated: neck left shoulder, right shoulder, right flank and left flank (**Figure 2B**). In **Figure 6** we show the mapping of the centroids to the surface of the RBD with the Omicon mutations shown as spikes, as expected there is correlation between the two although the antibody centroids are more broadly spread across the RBD surface, in particular there are no mutations in the left flank epitope, where a significant number of antibodies bind (**Figure 6A**). This information is also displayed mapped to the primary structure in **Figure 1A**. Left flank epitope antibodies can neutralize in some assays, and confer protection (Barnes et al., 2020; Dejnirattisai et al., 2021a) and this cryptic epitope might therefore be an important target for therapeutic antibody applications and cross-protective

vaccine antigen (Pinto et al., 2020). Nineteen of the 20 most potent (FRNT50<100ng/ml) neutralising monoclonal antibodies we isolated from early pandemic cases mapped to the ACE2 binding site across the neck and shoulder epitopes of the RBD and 5 of these classified as public IGVH3-53 antibodies (Dejnirattisai et al., 2021a; Yuan et al., 2020). Mapping these onto the RBD surface (**Figure 6B**) shows that the centroids are highly concentrated in the neck region. IGVH3-53 mAbs are especially common and although their centroid is at the neck they are orientated such that their light chain CDRs interact with the right shoulder (**Figure S3**). Most IGVH3-53 mAbs are sensitive to the N501Y mutation although some such as mAb 222 or Beta-27 can still neutralize 501Y containing viruses (Dejnirattisai et al., 2021b; Liu et al., 2021b) Omicron mutation Y505H makes a direct interaction with the L1 and L3 CDRs of mAb 222 (Dejnirattisai et al., 2021b). This will likely abolish binding across the board and Q493R may also impact interaction with the H3 loop.

MAb 253 as well as 55 and 165 are IGVH1-58 mAbs which bind an epitope shifted towards the left shoulder with H3 contacting S477N, although this mutation may not compromise binding (**Figure S3**) but Q493R may be disruptive in this case approaching the H2 CDR, however, the side-chain may fold back and not interfere with binding. MAbs 316, 88 and 384 all interact with E484 (mAb 316 via H1 and H2) within the left shoulder epitope. Here we would surmise that the E484A mutation would disrupt binding. In the case of mAb 316, Q493 makes direct interactions with H1 and H3, thus Q493R will also likely be deleterious. Broadly neutralizing mAb 58 binds at the front of the RBD reaching towards the right flank in an area which is relatively clear of mutations and thus may be unaffected (**Figure S3**). MAb 278 binds in a similar area but higher, the epitope comprising more of the right shoulder with L3 in

contact with G446; it is therefore plausible that G446S could interfere with binding (**Figure S3**).

MAb 170 will certainly be affected by Q493R and Q498R, which make direct interactions with L1 and H3 respectively (**Figure S3**). Q498R is between G496S and G446S (**Figure 4C**) and these substitutions may act in concert but since G446 is in proximity to H1 this is likely to impair interaction. The binding sites of selected potent antibodies including two which are cross-reactive against previous variants are shown in **Figure 7A**. We would expect all of these, with the exception of mAb58, to be affected by the mutations in Omicron.

Effect of Omicron mutations on Beta antibody responses

We have derived a panel of 27 potent Beta antibodies (FRNT <100 ng/ml) (Liu et al., 2021b) and this revealed a surprisingly skewed response with 18/27 potent antibodies targeting the Beta mutations: E484K, K417N and N501Y. This is seen in **Figure 6C**, where the focus on residues in the shoulders has spread the centroid patch out towards several Omicron mutation sites, this information is mapped to the primary structure in **Figure 1A**. Whilst K417N and N501Y are conserved in Omicron, E484 is mutated to an alanine, which seems a likely escape mutation to the Beta response to 484K. A large number of Beta mAbs that target 501Y will be compromised by Omicron mutations: N440K, G446S, Q493R, G496S, Q498R and Y505H including some public VH4-39 antibodies (Liu et al., 2021b). Beta MAbs targeting the back of the neck epitope (Beta-22,29,30) will be affected, for example in the case of Beta-29, H1 makes extensive interactions with residues Q493, G496 and Y505 (**Figure S4**). Beta-44 binding to the left shoulder epitope has already been shown to be sensitive to T478K whilst the combination of S477N and T478K in Omicron is likely to be more deleterious.

Four Beta-mAbs have been shown to potently cross-neutralize all Alpha, Beta, Gamma and Delta variants (Liu et al., 2021b), their binding sites are shown in **Figure 7B**.

Of these, Beta-27 is a VH3-53 antibody, which contacts Q493 and Y505 in a similar way to mAb222 and may thus be compromised. Beta-47, a VH1-58 antibody, binding towards the left shoulder epitope is not sensitive to T478K mutation, but having contacts with S477 and Q493 may still be affected, although pseudovirus Iota neutralization is preserved suggesting S477N is not important (**Figure S4, S2B**). Beta-49 and 50 similarly bind to the right flank epitope such that H3, directly above RDB G399, would be expected to clash with G399D. Their H3 also interacts with the N343 glycans whose conformation may be altered by the S371L and S373P mutations. Beta-53 also binds to the right flank with H1 contacting residue 339 and likely clashing with G339D and L1 will likely contact G446S so we might expect binding to be affected (**Figure S4**).

Effect of Omicron mutations on current antibody therapeutics

A number of individual antibodies or, cocktails of potently neutralizing antibodies (usually combinations recognizing different epitopes to avoid the likelihood of escape (Sun et al., 2021)) have been licensed for use and the aggregate of their binding shown in **Figure 6D** illustrates the strong correlation of aggregate binding with points of mutation and the attachment of each is shown schematically in **Figure 7C** and mapped to the primary structure in **Figure 1A**. More specifically:

Regeneron 10987 and 10933: Regeneron 10933 (Weinreich et al., 2021) binds the back of the left shoulder and 10987 the right shoulder (**Figure 7C, Figure S5**). It has already been shown

that REGN 10933 was unable to effectively neutralize Beta being sensitive to E484K (Zhou et al., 2021). REGN10933 H2 also contacts Q493 and is therefore likely to be severely compromised. REGN10987 H3 has direct contact with N440 and H2 with G446 and so this antibody is also likely to be affected (**Figure S5**).

Vir S309: S309 (Dejnirattisai et al., 2021a; Pinto et al., 2020; Sun and Ho, 2020) binds on the right flank with H3 contacting G339 and N343 glycans the latter close to the Serine 371, 373 and 375 mutations (**Figure S5**). Its binding could be affected.

AZD8895 & AZD1061: AZD8895 binds the left shoulder and AZD1061 the front of the right shoulder (**Figure S5**). We may hypothesize that AZD1061 would be affected due to contacts with the G446 loop (L2 and H3). AZD8895 a VH1-58 antibody like 253 & Beta-47, contacts S477 (H3) & Q493 (H2) and might be affected. However, neutralization data shows that IGVH1-58 antibodies are not affected by S477N change present in an Iota pseudovirus (**Figure S2B**).

LY-CoV016 and 555: LY-CoV016 is a VH3-53 antibody and has extensive interactions with Y505 via L1 and L3 making it likely vulnerable to mutations at this residue (**Figure S5**). LY-CoV555 (Sun and Ho, 2020) has been shown to be sensitive to the E484K mutation in delta (Liu et al., 2021a) and also contacts Q493 therefore this is likely to be compromised.

Discussion

The first 4 Omicron sequences were deposited on 24th November 2021, but many more cases have since been identified, corresponding to a large rise in cases in South Africa, and

indications from S gene drop out in the diagnostic PCR, suggest that it is already widespread in Southern Africa. Within days distant international spread has been seen in more than a dozen countries. Over the next weeks estimates of transmissibility, disease severity, vaccine efficacy and the ability of Omicron to evade natural and vaccine elicited antibody responses will become clearer.

The 34 individual changes (including deletions and insertions) found in Omicron S is extraordinary, previous variants of concern had far fewer Alpha 9; Beta 10; Gamma 12 and Delta 10. In all of these viruses the NTD, RBD and the furin cleavage site region have been hotspots for mutation (Zahradnik et al., 2021b) and within the RBD, mutation has concentrated on the ACE2 interacting surface and the right flank. There seem to be two main drivers for the evolution of the RBD; increasing affinity to ACE2 and escape from the antibody response.

Increasing affinity to ACE2 is likely to aid transmission, potentially reducing the infectious dose required or increasing the kinetics of viral replication in the infected host. Increased transmissibility becomes more important as herd immunity in the general population increases. The similarity of changes in the Omicron receptor-binding site to the *in vitro* evolved RBD-62 (Zahradnik et al., 2021b) is striking. Having acquired the cardinal RBD-62 mutations S477N, Q498R, N501Y as well as E484A (E484K in RBD-62, Beta and Gamma), it is likely that the affinity of Omicron RBD for ACE2 is substantially increased compared to Wuhan RBD or the Alpha, Beta, Gamma and Delta variants, driven by the crucial Q498R mutation and improved charge complementarity at the interaction interface with ACE2 (**Figure 4F**). We show here that the higher affinity ACE2 binders do not impair infection using a pseudoviral

system, likely because S1 is cleaved before S2 executes membrane fusion. We also show that although RBD-62 has an affinity higher than that of neutralizing mAbs, the neutralizing activity of monoclonal antibodies, still able to bind RBD-62 is not impaired, presumably because of the slow off rate for the mAb. Finally, if like RBD-62 Omicron promotes much increased syncytial formation (Rajah et al., 2021) this is a further mechanism to increase viral replication and immune avoidance.

Most potent neutralizing antibodies bind on, or in close proximity to the ACE2 footprint (neck and shoulder epitopes) and block interaction of S with ACE2, thereby preventing viral attachment to the host cell. There are two other classes of potent neutralizing mAb, firstly antibodies binding in close proximity to the N343 glycan (right flank epitope) exemplified by Vir S309(Pinto et al., 2020) and include the Beta 49, 50 and 53 antibodies (Liu et al., 2021b) used in our analysis. These mAbs bind distant from the ACE2 binding site, do not block ACE2 interaction and their mechanism of action may be to destabilize the S trimer. Finally, antibodies binding to the supersite on the NTD can also be potently neutralizing although the mechanism of action of NTD antibodies remains obscure (Cerutti et al., 2021; Chi et al., 2020; Dejnirattisai et al., 2021a). Multiple mutations at all three of these sites: the receptor binding site, proximal to N343 glycan and NTD are found in Omicron and likely point to a driver of immune evasion for their evolution. The left flank epitope, which is not mutated in Omicron, in contrast is used by antibodies that do not block ACE2 binding, are not classed as potently neutralising in some assays and yet have been shown to be protective in animal models(Barnes et al., 2020; Dejnirattisai et al., 2021a; Hastie et al., 2021). This epitope is inaccessible with the RBD in most conformations with binding proposed to destabilise the S trimer(Benton et al., 2020; Huo et al., 2020; Zhou et al., 2020) and is strongly conserved. It is

possible that structural constraints on this epitope may render escape more problematic and this may therefore be an important target.

In contrast, the concentration of potent neutralizing antibodies around the 25 amino acid receptor binding motif might suggest that this would be an Achilles heel for SARS-CoV-2, with ACE2 placing constraints on its variability (Rossmann et al., 1985), however the extraordinary plasticity of this site to absorb mutational change, whilst retaining affinity for ACE2 means rather than an Achilles heel, it is a potent weapon to evade the antibody response. Such camouflage of receptor binding sites has been observed before (see for example Acharya et al 1989 (Acharya et al., 1989)), but to a lesser extent, here it seems that the extremely advantageous Q498R mutation permits the virus to maintain fitness whilst enabling many other less energetically favorable changes, and hence fuels antigenic escape. Thus, by mutating the receptor binding site, the virus can both increase ACE2 affinity and potentially transmissibility, whist at the same time evading the antibody response.

Omicron may also have lost the ability to form the lipid binding pocket within the RBD which may normally aid release of the virus from infected cells, by a triplet of changes from serines to more bulky, hydrophobic residues, a motif not found in any of the other Sarbecoviruses. This may be significant to the trimer interaction and the presentation of the RBD, likely increasing the propensity for the RBD-up conformation (Gobeil et al., 2021). Since one of these mutations requires a double change in the codon it is likely that this effect is significant and it is conceivable that it acts in synergy with the change at residue 498, perhaps explaining why, even in the context of N501Y, present in Alpha, Beta, Gamma and other minor variants, this mutation has not established itself earlier. It has been predicted that increasing immunity

by natural infection or vaccination will increase the selective pressure to find a susceptible host, either by increased transmissibility or antibody evasion, it looks likely that Omicron has achieved both of these goals.

In the modelling presented above we show that almost every potent mAb makes some contact with mutated residues, slightly more so for the Beta mAbs suggesting that Omicron may have arisen to escape the Beta variant, in addition the change to Ala 484 is unusual and is most simply explained as escape from the 484K focussed responses to Beta. It therefore seems likely that Omicron evolved in a population without sequencing surveillance, in the face of prevalent Beta variant seroconversion. For many antibodies the changes in interaction are so severe that activity will likely be completely lost or severely impaired. This also extends to the set of mAbs developed for clinical use, the activity of most is likely to be lost or severely impaired. We will know when the virus is available how well these antibodies perform and there is hope that AZD8895 and Vir S309 may retain activity.

There are many unknowns about Omicron, chief is whether it will get a foothold and spread globally or whether it will behave like Beta, that looked likely to follow the path of Alpha but for some reason did not become a dominant strain outside Africa. If Omicron does spread it is likely that the increased affinity of its RBD for ACE2 and likely increased presentation of the RBD, will make it more transmissible and that there will be substantial reduction in the neutralizing capacity of vaccinated or naturally infected serum (**Figure S6**). Studies will be performed urgently to determine these parameters, but it is our opinion that neutralization will be knocked out in low titre serum whilst serum with higher starting titres is likely to retain some neutralizing capacity.

We have previously compared the neutralization of early pandemic SARS-CoV-2 strains, Alpha, Beta, Gamma and Delta using serum obtained early during the early pandemic or from Alpha, Beta or Gamma infected individuals. This allowed us to build a crude antigenic map of the SARS-CoV-2 sero-complex(Liu et al., 2021a). Early pandemic viruses and Alpha sit close to the centre, whilst Beta/Gamma diverge in one direction and Delta in the opposite direction, meaning that Beta/Gamma serum poorly neutralize Delta and vice versa. We expect that Omicron will occupy a substantially more distant position than Beta, Gamma and Delta with implications for vaccination programmes.

At present, the only option is to pursue vaccination with Wuhan containing antigen and ensure boosting of the response to high titres to provide some protection against Omicron. However, the antigenic distance of Omicron may mandate the development of vaccines against this strain. There will then be a question of how to use these vaccines; vaccination with Omicron will likely give good protection against Omicron, but will not give good protection against other strains. It seems possible therefore that Omicron may cause a shift from the current monovalent vaccines containing Wuhan S to multivalent vaccines containing an antigen such as Wuhan or Alpha at the centre of the antigenic map and Omicron or other S genes at the extreme peripheries of the map, similar to the polyvalent strategies used in influenza vaccines.

In summary, we have presented data showing that the huge number of mutational changes present in Omicron are likely to increase transmissibility and substantially knock down the neutralizing capacity of immune serum. This will likely lead to a fall in vaccine efficacy, but it

is unlikely that vaccines will completely fail and it is hoped that although vaccine breakthroughs will occur, protection from severe disease will be maintained, perhaps by T cells as it is likely that the vaccine induced T cell response to SARS-CoV-2 will be less affected than the antibody response. Widespread vaccine breakthrough may mandate the production of a vaccine tailored to Omicron and failure of monoclonal antibodies may likewise lead to the generation of second generation mAbs targeting Omicron.

A question asked after the appearance of each new variant is whether SARS-CoV-2 has reached its limit for evolution. Analysing the mutations in Omicron shows that, except for S371L, all other mutations required only single-nucleotide changes. Also, most changes observed in the *in vitro* evolution study constituted single-nucleotide mutations. Two-nucleotide mutations and epistatic mutations are more difficult to reach, but open up vast untapped potentials for future variants. To avoid this, one has to reduce the number of infected people through vaccination and other measures everywhere, not only in rich countries.

Limitations

Much of the data presented in this early study are modelled from existing data, there will be a need in the coming weeks to exemplify (or not) our predictions experimentally.

Acknowledgements

This work was supported by the Chinese Academy of Medical Sciences (CAMS) Innovation Fund for Medical Science (CIFMS), China (grant number: 2018-I2M-2-002) to D.I.S. and G.R.S.

H.M.E.D. and J.Ren are supported by the Wellcome Trust (101122/Z/13/Z), D.I.S. and E.E.F. by the UKRI MRC (MR/N00065X/1). G.S and J.Z were supported by the Israel Science Foundation (grant no. 3814/19) and O.A and S.K (grant no. 3729/20) within the KillCorona—Curbing Coronavirus Research Program and by the Ben B. and Joyce E. Eisenberg Foundation. D.I.S. and G.R.S. are Jenner Investigators. This is a contribution from the UK Instruct-ERIC Centre. The Wellcome Centre for Human Genetics is supported by the Wellcome Trust (grant 090532/Z/09/Z). The computational aspects of this research were supported by the Wellcome Trust Core Award Grant Number 203141/Z/16/Z and the NIHR Oxford BRC.

Author Information

These authors contributed equally: J.Z, A.T, H.G

Contributions

J.R., H.M.E.D, E.E.F. J.Z and D.I.S. analysed the structural results. G.R.S., J.M., P.S., Y.Z., D.Z., B.W., R.N., A.T., C.L., J.Z and D.Z. prepared S constructs, RBDs, ACE2 and mAbs and, C.L, W.D. P.S., R.N., and A.T. performed neutralization assays. J.Z and GS prepared RBD mutations and performed binding studies. O.A and S.K planned and performed syncytia studies. H.M.G. performed mapping and cluster analysis and sequence and antigenic space analyses. N.T. provided the SARS-CoV-2 lentiviral construct. G.R.S., G.S. and D.I.S. conceived the study, E.E.F, G.R.S. GS and D.I.S. wrote the initial manuscript draft with other authors providing editorial comments. All authors read and approved the manuscript

Competing Financial Interests

G.R.S sits on the GSK Vaccines Scientific Advisory Board and is a founder member of RQ Biotechnology. J.Z. and G.S. declare the Israel patent application no. 23/09/2020 – 277546 and U.S.A patent application no. 16/12/2020 - 63/125,984, entitled Methods and compositions for treating coronaviral infections.

Figure legends

Figure 1 Sarbecovirus RBD sequence analysis. Shown with Alpha, Beta, Delta and Omicron variants (the latter repeated on the lower line to clarify the Omicron changes. Binding sites for the early pandemic potent antibodies (Dejnirattisai et al., 2021a) and the potent Beta antibodies ((Liu et al., 2021b) are depicted using iron heat colours (grey > straw > blue > glowing red > yellow > white) to indicate relative levels of antibody contact and commercial antibody contacts are depicted with the pairs of antibodies in red or blue with purple denoting interactions with the same residue). Totally conserved residues are boxed on a red background on the upper rows, whilst on the final row the Omicron mutations are boxed in red. Secondary elements are denoted above the alignment. The figure was produced in part using Espript (Robert and Gouet, 2014). (B) Number of sequenced mutations per position. The line shows the number of mutations per residue, for high to low along the spike protein. In green are mutations D614G, which is fixed from early virus evolution and position 498, which became dominant only in omicron. Red are for mutations in Omicron that were identified before in multiple linages and blue are mutations with Omicron being the only lineage.

Figure 2 Distribution of Omicron changes. (A) Trimeric S model depicted as a grey surface with one monomer highlighted in pale blue, ACE2 binding site in green and changes in Omicron shown in red, left side view, right top view. (B) RBD depicted as a grey surface with

the ACE2 footprint in dark grey and changes in Omicron in red, left: top view, right: front and back views. Epitopes are labelled according to the torso analogy and mutations labelled. (C,D,E,F) Top view of RBD depicted as a grey surface with (C), ACE2 binding site in green (D), Alpha change in yellow (E), Beta changes in cyan (F), Delta changes in purple. Figure produced using chimera X (Pettersen et al., 2021).

Figure 3 Alphafold2 predicted Omicron Structures. (A) Left panel top ranked alphafold2 predicted Omicron RBD drawn as a red cartoon overlaid on the structure of the early pandemic (Wuhan) RBD (grey). The region consistently showing an altered conformation in the predicted models is enlarged right (red and grey cartoons) corresponding to the lipid pocket. It has been rotated for clarity and is superimposed on the corresponding region from the lipid bound RBD structure (green cartoon). The linoleic acid lipid is drawn in green sticks and the Omicron mutations giving rise to this change: S371L, S373P and S375F are marked by stars in the colour of the corresponding model. (B) Alphafold2 predicted model for the NTD (grey cartoon) superimposed on the 4A8 neutralising antibody/NTD complex. Omicron changes in the NTD are highlighted in red. (C) Alphafold2 predicted NTD structures (red cartoon) superimposed on early pandemic SARS-CoV-2 (grey cartoon) and SARS-CoV-1 (blue cartoon) structures.

Figure 4. Omicron S mutations have previously been identified by in vitro evolution for tighter binding. (A) Analysis of the occurrence and prevalence of Omicron variant mutations. The background is colored according to S-protein functional domains: NTD domain (AA 12 – 306; orange), RBD domain (AA 318 – 514; green), Furin cleavage site and its proximity (AA 655 – 701; blue). The four positions critical for the high affinity of RBD-62 are highlighted in bold.

Mutation frequencies within individual lineages are denoted in green (100-75 %), blue (75-50 %) and magenta (50-25 %). Information about the distribution and frequency of S-protein mutations and the spatiotemporal characterization of SARS-CoV-2 lineages was retrieved from www.outbreak.info (Mullen et al., 2020) and Gisaid database (Elbe and Buckland-Merrett, 2017).* Same evolutionary origin, a Number of evolutionary non-related lineages with given or similar mutation (Zahradnik et al., 2021c), b log(10) number of the observed Omicron mutation at the given position as determined on 14.11.2021, c same as b but total log(10) number of changes at the given position. d Log(10) change in binding as determined from deep mutational scanning (Starr et al., 2020). (B) Comparison of fold change in binding affinity among selected mutations and their combinations. Some of the values have been reported previously (Zahradnik et al., 2021b). e Yellow mutations are from Starr et al., 2020(Starr et al., 2020). (C) RBD-62/ACE2 structure with the breakdown of Omicron mutations: Red mutations are the same for RBD-62 and Omicron variant RBD. Orange highlights mutations not present in the RBD-62 but sampled by yeast display affinity maturation. Yellow mutations are unique for the Omicron variant. The mutations were drawn on the template of the RBD-62 – ACE2 structure (PDB ID: 7BH9). (D) Detail of interaction between S477N and S19 of ACE2. (E) Details of selected interactions contributing to the higher affinity of RBD containing Q498R+N501Y. The Omicron-specific mutation G496S may further contribute to this network of interactions. (F) Electrostatic potential surface depictions calculated using the APBS plugin in PyMol for left to right: early pandemic Victoria (close to Wuhan) RBD showing the ACE2 interacting surface, ACE2 showing surface that binds the RBD, Beta RBD ACE2 interacting surface, RBD-62 ACE2 interacting surface, Omicron RBD ACE2 interacting surface. Blue is positive and red negative potential (scale bar shown above).

Figure 5. Extreme affinity RBD-62 introduced in Spike protein led increase in syncytia formation. Syncytia formation analysis in HEK293T stably over-expressing human TMPRSS2 and ACE2 seeded on imaging plates. Cells plasma membranes were stained with CellMask Deep Red (magenta) and nuclei were stained with Hoechst 33342 (yellow) 24 hours after transfection.

Figure 6. Relative Antibody Contact. RBD surface rendered in PyMOL exported and rendered in mabscape using iron heat colours (grey > straw > blue > glowing red > yellow > white) to indicate relative levels of antibody contact. Antibody contact is calculated for each surface vertex as the number of antibodies within a 10 Å radius by their known or predicted positions from earlier mapping studies (Dejnirattisai et al., 2021a; Liu et al., 2021b). Outward facing cones are placed at the nearest vertex to each mutated residue Calpha atom on the RBD surface. Drawn back and front views for (A) all RBD-reactive antibodies isolated from early pandemic or strongly neutralizing (< 100 ng/ml) (B) strongly neutralising antibodies isolated from Beta-infected sera (C) therapeutic antibodies for clinical use (from PDB codes: 7BEP, 6XDG, 7L7E, 7KMG, 7KMH).

Figure 7 Correlation of mutations and antibody footprints. (A,B,C) Front (left) and back (right) views of the RBD drawn as a grey surface with Omicron changes highlighted in magenta and glycans drawn as sticks. (A) Outline footprints of a selection of early pandemic mAbs: 58, 88, 222, 253, 278 are shown by balls representing the centroid of interacting loops for LC (blues), HC (reds) and joined by yellow lines. (B) As for A, showing a selection of Beta antibodies:27, 47, 49, 53. Substituted residues in magenta are labelled. (C) As for A showing

the footprints of a selection of commercial antibodies: REGN10933, REGN10987, S309, AZD1061, AZD8895, LY-CoV555, LY-CoV016.

STAR Methods

RESOURCE AVAILABILITY

Lead Contact

Resources, reagents and further information requirement should be forwarded to and will be responded by the Lead Contact, David I Stuart (dave@strubi.ox.ac.uk).

Materials Availability

Reagents generated in this study are available from the Lead Contact with a completed Materials Transfer Agreement.

Data and Code Availability

- Any additional information required to re-analyze the data reported in this paper is available from the lead contact upon request.

EXPERIMENTAL MODEL AND SUBJECT DETAILS

Transduction of Pseudotyped Lentivirus in human ACE2 stable cell line

Production of luciferase reporter pesudotyped lentiviral particles expressing SARS-CoV-2 S protein was carried out as described previously (Di Genova et al., 2020). The resulting pseudoviral particles of RBD mutation (PV-RBD-62) and wild type (PV-Wuhan) were normalized based on the level of p24 antigen using RETROtek HIV-1 p24 Antigen-ELISA kit (Zeptometrix; Buffalo, NY), according to the manufacturer's instructions. A series of 3-fold dilutions of PV-RBD-62 or Wuhan were prepared, separately, prior to transduction into human ACE2 receptor expressing HEK293T/17 stable cell line grown on white opaque 96-well

microplates. 48h post transduction, culture supernatants were removed and 50 µL of 1:2 Bright-GloTM Luciferase assay reagent (Promega, USA) in 1x PBS was added to each well. The reaction was incubated at room temperature for 5 mins and the firefly luciferase activity was measured using CLARIOstar® (BMG Labtech, Ortenberg, Germany). The relative light unit (RLU) reflecting the transduction ability of PV-RBD and PV-Wuhan were then compared.

Pseudoviral neutralization test

The details of pseudoviral neutralization test as were described previously (Liu et al., 2021a) with some modifications. Briefly, neutralizing activity of anti-RBD or -NTD monoclonal antibodies (mAbs) isolated during the early pandemic in UK were tested against PV-RBD-62 together with wild type (PV-Wuhan). A 4-fold serial dilution of each mAb was incubated with pseudoviral particles at 37˚C, 5% CO2 for 1 hr. The stable HEK293T/17 cells expressing human ACE2 were then added to the mixture at 1.5 x 10^4 cells/well and incubated for another 48 hrs prior to measuring the luciferase values. The percentage of mAb neutralization towards PV-RBD-62 or PV-Wuhan was calculated relative to the control. Probit analysis was used to estimate the value of dilution that inhibits half of the maximum pseudotyped lentivirus infection (PVNT50).

DNA manipulations

Cloning was done by using a restriction-free approach(Peleg and Unger, 2014). Mutagenic megaprimers were PCR amplified (KAPA HiFi HotStart ReadyMix, Roche, Switzerland, cat. KK3605), purified by using NucleoSpin® Gel and PCR Clean-up kit (Nacherey-Nagel, Germany, REF 740609.50) and cloned into pJYDC1 (Adgene ID: 162458) (Zahradnik et al., 2021a). Parental pJYDC1 molecules were cleaved by DpnI treatment (1 h, NEB, USA, cat. R0176) and

the reaction mixture was electroporated into E.coli Cloni® 10G cells (Lucigen, USA). The correctness of mutagenesis was verified by sequencing.

Yeast display binding assays

Plasmids (pJYDC1) with mutations were transformed (1 ug of DNA) by LiAc method(Gietz and Woods, 2006) into the EBY100 Saccharomyces cerevisiae and selected by growth on SD-W plates (Zahradnik et al., 2021a) for 48-72 h at 30°C. Grown single colonies were transferred to 1.0 ml liquid SD-CAA media, grown overnight at 30°C (220 rpm), and 50 ul of the starter culture was used as inoculum (5 %) for the expression culture in 1/9 media (1 ml) supplemented with 1 nM DMSO solubilized bilirubin (Merck/Sigma-Aldrich cat. B4126). The expression continued in a shaking incubator for 24 h at 20°C (220 rpm). Aliquots of yeast expressed cells (100 ul, 3000 g, 3 min) were washed in ice-cold PBSB buffer (PBS with 1 g/L BSA) and resuspended in PBSB with a dilution series CF640-ACE2 (1 pM – 50 nM). The volume and incubation times were adjusted to limit the ligand depletion effect and enable equilibrium (Zahradnik et al., 2021b). After incubation, cells were washed in ice-cold PBSB buffer (PBS with 1 g/L BSA) passed through cell strainer nylon membrane (40 µM, SPL Life Sciences, Korea), and analyzed. The signals for expression (FL1, eUnaG2 fluorophore, Ex. 498 nm, Em. 527 nm) and for binding (FL3, CF®640R dye-labeled ACE2) were recorded by S3e Cell Sorter (BioRad, USA). The standard non-cooperative Hill equation was fitted by nonlinear least-squares regression with two additional parameters using Python 3.7 (Starr et al., 2020; Zahradnik et al., 2021a).

Cell-Cell Fusion Assay

HEK293T stably over-expressing human TMPRSS2 and ACE2 were seeded on imaging plates at a density of 570 cells/mm2. 4 hours post-seeding, plasmids pcDNA3.1 containing the human optimized Spike protein or its variants under the control of CMV promoter were transfected at 1ug/ml. To calculate the number of nuclei per cell, cells were stained with CellMask Deep Red (ThermoFisher Scientific, 1:1000 dilution) for the plasma membrane and Hoechst 33342 (1:1000 dilution) for nuclei, 24 hours after transfection. The plates were imaged using a Yokogawa automatic Spinning Disk confocal scanning unit (CSU-W1-T2) mounted on an inverted Olympus IX83 microscope. 60x 1.4 NA oil immersion objective was used for data acquisition. Images were captured by a back-illuminated Prime 95B sCMOS camera (Photometrics), controlled by VisView software (Visitron Systems GmbH). The following fluorescence excitation and emission filter sets were used: 405 nm and 460/50 nm for Hoechst 33342, and 640 nm and 700/75 nm for CellMask Deep Red. The images were analyzed to calculate the fusion indices of the respective constructs.

Alphafold

Models of Omicron RBD and NTD were derived using AlphaFold 2.0.01(Jumper et al., 2021) downloaded and installed on 11th August 2021 in batch mode. For RBD predictions, 204 residues (P327-n529) were used as an input sequence while the NTD sequence input was from residues V1-S253. The max_release_date parameter was set to 28-11-2021 when the simulations were run such that template information was used for structure modelling. For all targets, five models were generated and all presets were kept the same.

QUANTIFICATION AND STATISTICAL ANALYSIS

Statistical analyses are reported in the results and figure legends. Neutralization was measured by FRNT. The percentage of focus reduction was calculated and IC_{50} (FRNT50) was determined using the probit program from the SPSS package. The Wilcoxon matched-pairs signed rank test was used for the analysis and two-tailed P values were calculated on geometric mean values.

References

Acharya, R., Fry, E., Stuart, D., Fox, G., Rowlands, D., and Brown, F. (1989). The three-dimensional structure of foot-and-mouth disease virus at 2.9 A resolution. Nature *337*, 709-716.

Barnes, C.O., Jette, C.A., Abernathy, M.E., Dam, K.A., Esswein, S.R., Gristick, H.B., Malyutin, A.G., Sharaf, N.G., Huey-Tubman, K.E., Lee, Y.E.*, et al.* (2020). SARS-CoV-2 neutralizing antibody structures inform therapeutic strategies. Nature *588*, 682-687.

Baum, A., Fulton, B.O., Wloga, E., Copin, R., Pascal, K.E., Russo, V., Giordano, S., Lanza, K., Negron, N., Ni, M.*, et al.* (2020). Antibody cocktail to SARS-CoV-2 spike protein prevents rapid mutational escape seen with individual antibodies. Science *369*, 1014-1018.

Benton, D.J., Wrobel, A.G., Xu, P., Roustan, C., Martin, S.R., Rosenthal, P.B., Skehel, J.J., and Gamblin, S.J. (2020). Receptor binding and priming of the spike protein of SARS-CoV-2 for membrane fusion. Nature *588*, 327-330.

Borges, V., Isidro, J., Cunha, M., Cochicho, D., Martins, L., Banha, L., Figueiredo, M., Rebelo, L., Trindade, M.C., Duarte, S.*, et al.* (2021). Long-Term Evolution of SARS-CoV-2 in an Immunocompromised Patient with Non-Hodgkin Lymphoma. mSphere *6*, e0024421.

Cerutti, G., Guo, Y., Zhou, T., Gorman, J., Lee, M., Rapp, M., Reddem, E.R., Yu, J., Bahna, F., Bimela, J.*, et al.* (2021). Potent SARS-CoV-2 neutralizing antibodies directed against spike N-terminal domain target a single supersite. Cell Host Microbe *29*, 819-833 e817.

Chi, X., Yan, R., Zhang, J., Zhang, G., Zhang, Y., Hao, M., Zhang, Z., Fan, P., Dong, Y., Yang, Y.*, et al.* (2020). A neutralizing human antibody binds to the N-terminal domain of the Spike protein of SARS-CoV-2. Science *369*, 650-655.

Colmenares-Mejia, C.C., Serrano-Diaz, N., Quintero-Lesmes, D.C., Meneses, L., Salazar Acosta, I., Idrovo, A.J., Sanabria-Echeverry, D.Y., Cordero-Rebolledo, H., and Castillo, V. (2021). Seroprevalence of SARS-CoV-2 Infection among Occupational Groups from the Bucaramanga Metropolitan Area, Colombia. Int J Environ Res Public Health *18*.

Dejnirattisai, W., Zhou, D., Ginn, H.M., Duyvesteyn, H.M.E., Supasa, P., Case, J.B., Zhao, Y., Walter, T.S., Mentzer, A.J., Liu, C.*, et al.* (2021a). The antigenic anatomy of SARS-CoV-2 receptor binding domain. Cell *184*, 2183-2200 e2122.

Dejnirattisai, W., Zhou, D., Supasa, P., Liu, C., Mentzer, A.J., Ginn, H.M., Zhao, Y., Duyvesteyn, H.M.E., Tuekprakhon, A., Nutalai, R.*, et al.* (2021b). Antibody evasion by the P.1 strain of SARS-CoV-2. Cell *184*, 2939-2954 e2939.

Di Genova, C., Sampson, A., Scott, S., Cantoni, D., Mayora-Neto, M., Bentley, E., Mattiuzzo, G., Wright, E., Derveni, M., Auld, B.*, et al.* (2020). Production, titration, neutralisation and storage of SARS-CoV-2 lentiviral pseudotypes. figshare.

Dong, J., Zost, S., Greaney, A., Starr, T.N., Dingens, A.S., Chen, E.C., Chen, R., Case, B., Sutton, R., Gilchuk, P.*, et al.* (2021). Genetic and structural basis for recognition of SARS-CoV-2 spike protein by a two-antibody cocktail. bioRxiv.

Elbe, S., and Buckland-Merrett, G. (2017). Data, disease and diplomacy: GISAID's innovative contribution to global health. Glob Chall *1*, 33-46.

Escalera, A., Gonzalez-Reiche, A.S., Aslam, S., Mena, I., Pearl, R.L., Laporte, M., Fossati, A., Rathnasinghe, R., Alshammary, H., van de Guchte, A.*, et al.* (2021). SARS-CoV-2 variants of concern have acquired mutations associated with an increased spike cleavage. bioRxiv, 2021.2008.2005.455290.

Gao, X., Qin, B., Chen, P., Zhu, K., Hou, P., Wojdyla, J.A., Wang, M., and Cui, S. (2021). Crystal structure of SARS-CoV-2 papain-like protease. Acta Pharm Sin B *11*, 237-245.

Gao, Y., Yan, L., Huang, Y., Liu, F., Zhao, Y., Cao, L., Wang, T., Sun, Q., Ming, Z., Zhang, L.*, et al.* (2020). Structure of the RNA-dependent RNA polymerase from COVID-19 virus. Science *368*, 779-782.

Gietz, R.D., and Woods, R.A. (2006). Yeast transformation by the LiAc/SS Carrier DNA/PEG method. Methods Mol Biol *313*, 107-120.

Gobeil, S.M., Janowska, K., McDowell, S., Mansouri, K., Parks, R., Stalls, V., Kopp, M.F., Manne, K., Li, D., Wiehe, K.*, et al.* (2021). Effect of natural mutations of SARS-CoV-2 on spike structure, conformation, and antigenicity. Science *373*.

Hastie, K.M., Li, H., Bedinger, D., Schendel, S.L., Dennison, S.M., Li, K., Rayaprolu, V., Yu, X., Mann, C., Zandonatti, M.*, et al.* (2021). Defining variant-resistant epitopes targeted by SARS-CoV-2 antibodies: A global consortium study. Science *374*, 472-478.

Huo, J., Zhao, Y., Ren, J., Zhou, D., Duyvesteyn, H.M.E., Ginn, H.M., Carrique, L., Malinauskas, T., Ruza, R.R., Shah, P.N.M.*, et al.* (2020). Neutralization of SARS-CoV-2 by Destruction of the Prefusion Spike. Cell Host Microbe.

Jumper, J., Evans, R., Pritzel, A., Green, T., Figurnov, M., Ronneberger, O., Tunyasuvunakool, K., Bates, R., Zidek, A., Potapenko, A.*, et al.* (2021). Highly accurate protein structure prediction with AlphaFold. Nature.

Lan, J., Ge, J., Yu, J., Shan, S., Zhou, H., Fan, S., Zhang, Q., Shi, X., Wang, Q., Zhang, L.*, et al.* (2020). Structure of the SARS-CoV-2 spike receptor-binding domain bound to the ACE2 receptor. Nature *581*, 215-220.

Liu, C., Ginn, H.M., Dejnirattisai, W., Supasa, P., Wang, B., Tuekprakhon, A., Nutalai, R., Zhou, D., Mentzer, A.J., Zhao, Y.*, et al.* (2021a). Reduced neutralization of SARS-CoV-2 B.1.617 by vaccine and convalescent serum. Cell *184*, 4220-4236 e4213.

Liu, C., Zhou, D., Nutalai, R., Duyvestyn, H., Tuekprakhon, A., Ginn, H., Dejnirattisai, W., Supasa, P., Mentzer, A., Wang, B.*, et al.* (2021b). The Beta mAb response underscores the antigenic distance to other SARS-CoV-2

variants. Cell, Host and Microbe.

Liu, Y., Soh, W.T., Kishikawa, J.I., Hirose, M., Nakayama, E.E., Li, S., Sasai, M., Suzuki, T., Tada, A., Arakawa, A.*, et al.* (2021c). An infectivity-enhancing site on the SARS-CoV-2 spike protein targeted by antibodies. *184*, 3452-3466 e3418.

Martin, D.P., Weaver, S., Tegally, H., San, J.E., Shank, S.D., Wilkinson, E., Lucaci, A.G., Giandhari, J., Naidoo, S., Pillay, Y.*, et al.* (2021). The emergence and ongoing convergent evolution of the SARS-CoV-2 N501Y lineages. Cell *184*, 5189-5200 e5187.

Mlcochova, P., Kemp, S.A., Dhar, M.S., Papa, G., Meng, B., Ferreira, I., Datir, R., Collier, D.A., Albecka, A., Singh, S.*, et al.* (2021). SARS-CoV-2 B.1.617.2 Delta variant replication and immune evasion. Nature *599*, 114-119.

Moeller, N.H., Shi, K., Demir, O., Banerjee, S., Yin, L., Belica, C., Durfee, C., Amaro, R.E., and Aihara, H. (2021). Structure and dynamics of SARS-CoV-2 proofreading exoribonuclease ExoN. bioRxiv.

Mullen, J.L., Tsueng, G., Latif, A.A., Alkuzweny, M., Cano, M., Haag, E., Zhou, J., Zeller, M., Hufbauer, E., Matteson, N.*, et al.* (2020). Center for Viral Systems Biology outbreak.info.

Owen, D.R., Allerton, C.M.N., Anderson, A.S., Aschenbrenner, L., Avery, M., Berritt, S., Boras, B., Cardin, R.D., Carlo, A., Coffman, K.J.*, et al.* (2021). An oral SARS-CoV-2 M(pro) inhibitor clinical candidate for the treatment of COVID-19. Science, eabl4784.

Peleg, Y., and Unger, T. (2014). Application of the Restriction-Free (RF) cloning for multicomponents assembly. Methods Mol Biol *1116*, 73-87.

Pettersen, E.F., Goddard, T.D., Huang, C.C., Meng, E.C., Couch, G.S., Croll, T.I., Morris, J.H., and Ferrin, T.E. (2021). UCSF ChimeraX: Structure visualization for researchers, educators, and developers. Protein Sci *30*, 70-82.

Pinto, D., Park, Y.J., Beltramello, M., Walls, A.C., Tortorici, M.A., Bianchi, S., Jaconi, S., Culap, K., Zatta, F., De Marco, A.*, et al.* (2020). Cross-neutralization of SARS-CoV-2 by a human monoclonal SARS-CoV antibody. Nature *583*, 290-295.

Plante, J.A., Liu, Y., Liu, J., Xia, H., Johnson, B.A., Lokugamage, K.G., Zhang, X., Muruato, A.E., Zou, J., Fontes-Garfias, C.R.*, et al.* (2021). Spike mutation D614G alters SARS-CoV-2 fitness. Nature *592*, 116-121.

Rajah, M.M., Hubert, M., Bishop, E., Saunders, N., Robinot, R., Grzelak, L., Planas, D., Dufloo, J., Gellenoncourt, S., Bongers, A.*, et al.* (2021). SARS-CoV-2 Alpha, Beta, and Delta variants display enhanced Spike-mediated syncytia formation. EMBO J, e108944.

Rambaut, A., Holmes, E.C., O'Toole, A., Hill, V., McCrone, J.T., Ruis, C., du Plessis, L., and Pybus, O.G. (2020). A dynamic nomenclature proposal for SARS-CoV-2 lineages to assist genomic epidemiology. Nat Microbiol *5*, 1403-1407.

Rapp, M., Guo, Y., Reddem, E.R., Yu, J., Liu, L., Wang, P., Cerutti, G., Katsamba, P., Bimela, J.S., Bahna, F.A.*, et al.* (2021). Modular basis for potent SARS-CoV-2 neutralization by a prevalent VH1-2-derived antibody class. Cell Rep *35*, 108950.

Robert, X., and Gouet, P. (2014). Deciphering key features in protein structures with the new ENDscript server. Nucleic Acids Res *42*, W320-324.

Rossmann, M.G., Arnold, E., Erickson, J.W., Frankenberger, E.A., Griffith, J.P., Hecht, H.J., Johnson, J.E., Kamer, G., Luo, M., Mosser, A.G.*, et al.* (1985). Structure of a human common cold virus and functional relationship to other picornaviruses. Nature *317*, 145-153.

Saito, A., Irie, T., Suzuki, R., Maemura, T., Nasser, H., Uriu, K., Kosugi, Y., Shirakawa, K., Sadamasu, K., Kimura, I.*, et al.* (2021). Enhanced fusogenicity and pathogenicity of SARS-CoV-2 Delta P681R mutation. Nature.

Starr, T.N., Greaney, A.J., Dingens, A.S., and Bloom, J.D. (2021). Complete map of SARS-CoV-2 RBD mutations that escape the monoclonal antibody LY-CoV555 and its cocktail with LY-CoV016. bioRxiv.

Starr, T.N., Greaney, A.J., Hilton, S.K., Ellis, D., Crawford, K.H.D., Dingens, A.S., Navarro, M.J., Bowen, J.E., Tortorici, M.A., Walls, A.C.*, et al.* (2020). Deep Mutational Scanning of SARS-CoV-2 Receptor Binding Domain Reveals Constraints on Folding and ACE2 Binding. Cell *182*, 1295-1310 e1220.

Sun, Y., and Ho, M. (2020). Emerging antibody-based therapeutics against SARS-CoV-2 during the global pandemic. Antib Ther *3*, 246-256.

Sun, Y., Wang, L., Feng, R., Wang, N., Wang, Y., Zhu, D., Xing, X., Yang, P., Zhang, Y., Li, W.*, et al.* (2021). Structure-based development of three- and four-antibody cocktails against SARS-CoV-2 via multiple mechanisms. Cell Res *31*, 597-600.

Supasa, P., Zhou, D., Dejnirattisai, W., Liu, C., Mentzer, A.J., Ginn, H.M., Zhao, Y., Duyvesteyn, H.M.E., Nutalai, R., Tuekprakhon, A.*, et al.* (2021). Reduced neutralization of SARS-CoV-2 B.1.1.7 variant by convalescent and vaccine sera. Cell *184*, 2201-2211 e2207.

Toelzer, C., Gupta, K., Yadav, S.K.N., Borucu, U., Davidson, A.D., Kavanagh Williamson, M., Shoemark, D.K., Garzoni, F., Staufer, O., Milligan, R.*, et al.* (2020). Free fatty acid binding pocket in the locked structure of SARS-CoV-2 spike protein. Science *370*, 725-730.

Valesano, A.L., Rumfelt, K.E., Dimcheff, D.E., Blair, C.N., Fitzsimmons, W.J., Petrie, J.G., Martin, E.T., and Lauring, A.S. (2021). Temporal dynamics of SARS-CoV-2 mutation accumulation within and across infected hosts. PLoS Pathog *17*, e1009499.

Walls, A.C., Park, Y.J., Tortorici, M.A., Wall, A., McGuire, A.T., and Veesler, D. (2020). Structure, Function, and Antigenicity of the SARS-CoV-2 Spike Glycoprotein. Cell *181*, 281-292 e286.

Walls, A.C., Tortorici, M.A., Snijder, J., Xiong, X., Bosch, B.J., Rey, F.A., and Veesler, D. (2017). Tectonic conformational changes of a coronavirus spike glycoprotein promote membrane fusion. Proc Natl Acad Sci U S A *114*, 11157-11162.

Weinreich, D.M., Sivapalasingam, S., Norton, T., Ali, S., Gao, H., Bhore, R., Musser, B.J., Soo, Y., Rofail, D., Im, J.*, et al.* (2021). REGN-COV2, a Neutralizing Antibody Cocktail, in Outpatients with Covid-19. N Engl J Med *384*, 238-251.

Wong, L.Y., Zheng, J., Wilhelmsen, K., Li, K., Ortiz, M.E., Schnicker, N.J., Pezzulo, A.A., Szachowicz, P.J., Klumpp, K., Aswad, F.*, et al.* (2021). Eicosanoid signaling as a therapeutic target in middle-aged mice with severe COVID-19. bioXriv.

Yuan, M., Liu, H., Wu, N.C., Lee, C.D., Zhu, X., Zhao, F., Huang, D., Yu, W., Hua, Y., Tien, H.*, et al.* (2020). Structural basis of a shared antibody response to SARS-CoV-2. Science *369*, 1119-1123.

Zahradnik, J., Dey, D., Marciano, S., Kolarova, L., Charendoff, C.I., Subtil, A., and Schreiber, G. (2021a). A Protein-Engineered, Enhanced Yeast Display Platform for Rapid Evolution of Challenging Targets. ACS Synth Biol.

Zahradnik, J., Marciano, S., Shemesh, M., Zoler, E., Harari, D., Chiaravalli, J., Meyer, B., Rudich, Y., Li, C., Marton, I.*, et al.* (2021b). SARS-CoV-2 variant prediction and antiviral drug design are enabled by RBD in vitro evolution. Nat Microbiol *6*, 1188-1198.

Zahradnik, J., Nunvar, J., and Schreiber, G. (2021c). SARS-CoV-2 convergent evolution as a guide to explore adaptive advantage. bioRxiv.

Zhou, D., Dejnirattisai, W., Supasa, P., Liu, C., Mentzer, A.J., Ginn, H.M., Zhao, Y., Duyvesteyn, H.M.E., Tuekprakhon, A., Nutalai, R.*, et al.* (2021). Evidence of escape of SARS-CoV-2 variant B.1.351 from natural and vaccine-induced sera. Cell *184*, 2348-2361 e2346.

Zhou, D., Duyvesteyn, H.M.E., Chen, C.P., Huang, C.G., Chen, T.H., Shih, S.R., Lin, Y.C., Cheng, C.Y., Cheng, S.H., Huang, Y.C.*, et al.* (2020). Structural basis for the neutralization of SARS-CoV-2 by an antibody from a convalescent patient. Nature structural & molecular biology *27*, 950-958.

Zost, S.J., Gilchuk, P., Case, J.B., Binshtein, E., Chen, R.E., Nkolola, J.P., Schafer, A., Reidy, J.X., Trivette, A., Nargi, R.S.*, et al.* (2020). Potently neutralizing and protective human antibodies against SARS-CoV-2. Nature *584*, 443-449.

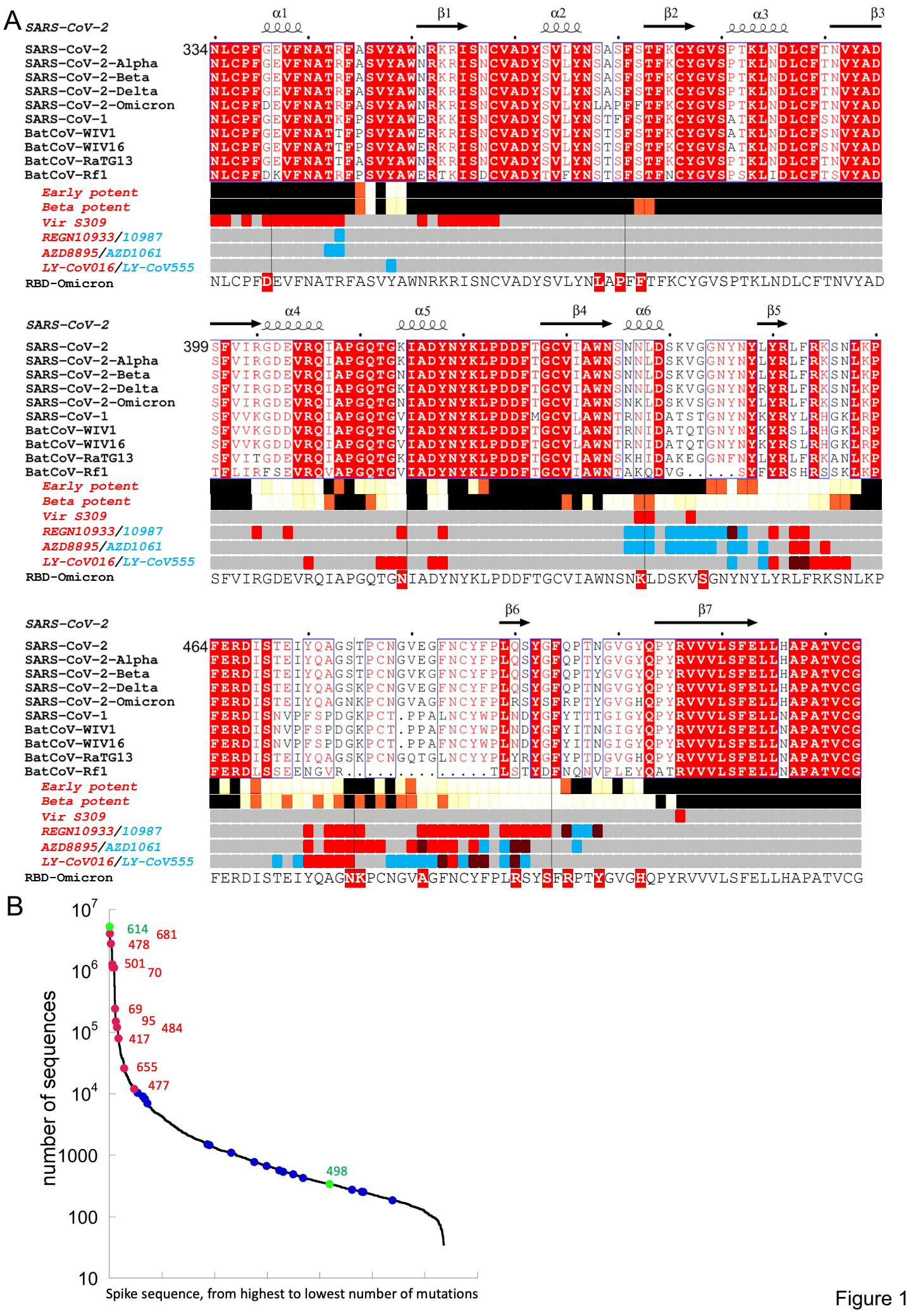
A
SARS-CoV-2
α1 β1 α2 β2 α3 β3
SARS-CoV-2
SARS-CoV-2-Alpha
SARS-CoV-2-Beta
SARS-CoV-2-Delta
SARS-CoV-2-Omicron
SARS-CoV-1
BatCoV-WIV1
BatCoV-WIV16
BatCoV-RaTG13
BatCoV-Rf1
Early potent
Beta potent
Vir S309
REGN10933/10987
AZD8895/AZD1061
LY-CoV016/LY-CoV555
RBD-Omicron
α4 α5 β4 α6 β5
β6 β7
B
number of sequences
Spike sequence, from highest to lowest number of mutations
614
681
478
501
70
69
95
484
417
655
477
498

Figure 1

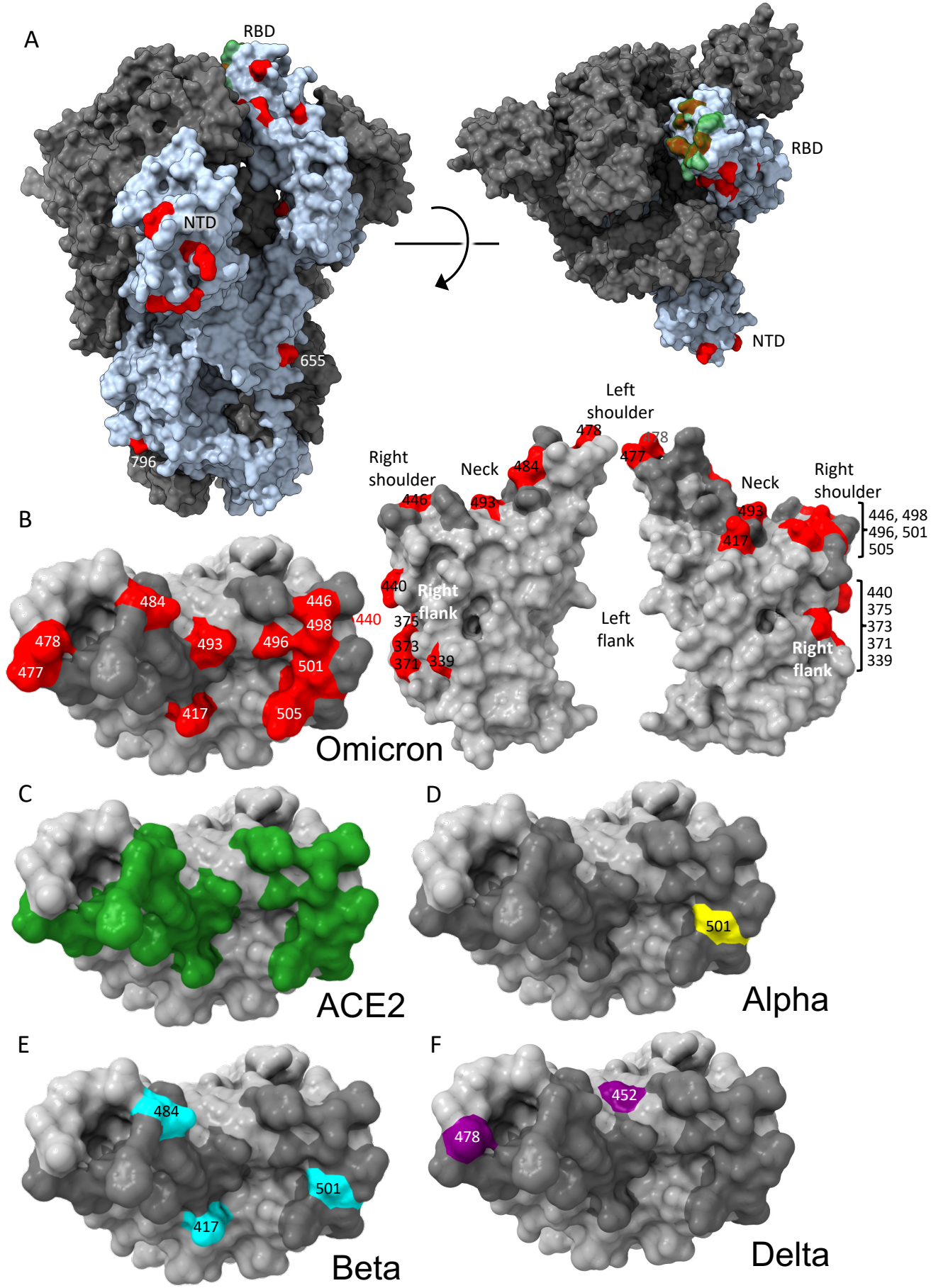
A
RBD
NTD
655
796
RBD
NTD
B
Left shoulder
478
478
477
Right shoulder
446
Neck
484
493
Neck
Right shoulder
493
417
446, 498
496, 501
505
440
Right flank
375
373
371
339
Left flank
Right flank
440
375
373
371
339
484
446
498
440
478
493
496
477
501
417
505
Omicron
C
ACE2
D
501
Alpha
E
484
501
417
Beta
F
452
478
Delta

Figure 2

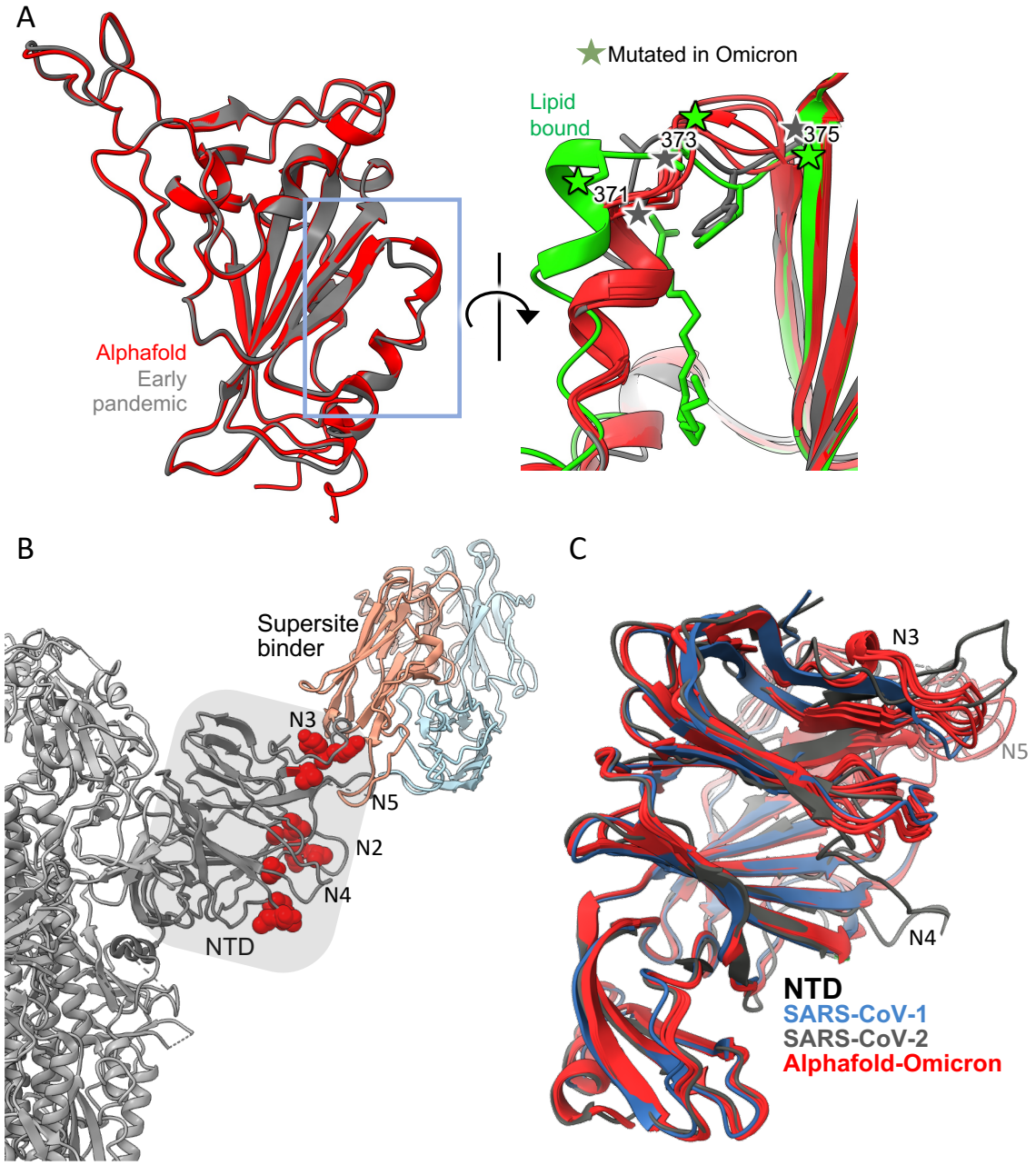
A
Mutated in Omicron
Lipid
bound
373
375
371
Alphafold
Early
pandemic
B
Supersite
binder
N3
N5
N2
N4
NTD
C
N3
N5
N4
NTD
SARS-CoV-1
SARS-CoV-2
Alphafold-Omicron

Figure 3

A

PANGO lineage	Alternative lineage identifier	Geographic prominence/ origin	A67	V69-70	T95	141-5	210-215	G339	S371	S373	S375	K417	N440	G446	S477	T478	E484	Q493	G496	Q498	N501	Y505	T547	D614	H655	N679	P681	N764	D796	N856	Q954	N969	L981
Original SARS-CoV-2 S-protein residue																																	
yeast display/**RBD-62**														R	**N**	S	**K**	H		**R**	**Y**												
B.1.1.529	omicron	South Africa	V	Δ	I	D	ins	D	L	P	F	N	K	S	N	K	A	R	S	R	Y	H	K	G	Y	K	H	K	Y	K	H	K	F
B.1.617.1	kappa	India			I	D*											Q							G			R#						
P.3	theta	Philippines				Δ											K				Y			G			H						
B.1.617.2	delta	India			I	D*										K								G			R#						
B.1.1.7	alpha	Europe		Δ																	Y			G			H						
P.1/4	gamma	Brazil										T					K				Y			G	Y								
B.1.351	beta	South Africa					G					N					K				Y			G									
B.1.525	eta	Central Africa	V	Δ													K							G									
B.1.526	iota	U.S., Ecuador			I#												K							G									
B.1.429/427	epsilon	U.S.																						G									
AA parallelism score [a]			2	8	8	24	9	1	1	1	1	3	1	1	9	6	17	1	1	1	14	1	1	*	7	1	17	1	4	1	1	1	1
GISAID no. of mutations (log 10) [b]			4.3	6.1	6.1	-	-	2.7	1.1	2.5	2.3	4.6	4.0	2.8	4.8	6.4	3.0	2.4	2.7	2.1	6.1	2.2	2.8	6.7	5.1	3.7	6.1	2.6	3.6	1.8	1.5	1.9	1.7
no of changes at position (log 10) [c]			4.4	6.1	6.1	-	-	3.0	2.7	3.2	2.6	5.2	4.0	4.0	4.9	6.4	5.4	3.2	2.8	2.5	6.1	2.4	3.9	6.7	5.1	3.8	6.6	2.7	4.1	3.0	2.7	2.4	2.3
Log(10) fold-change in binding [d]			-	-	-	-	-	-	-0.14	-0.08	-0.55	-0.45	0.07	-0.2	0.06	0.02	-0.07	-0.09	-0.63	-0.06	0.24	-0.71	-	-	-	-	-	-	-	-	-	-	-

B

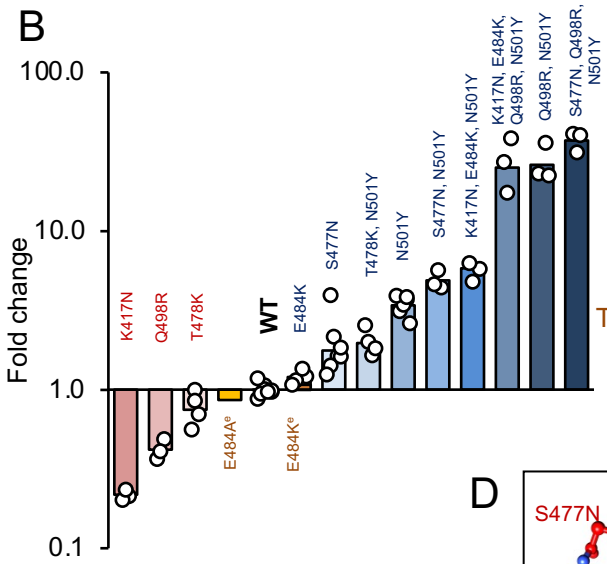

C

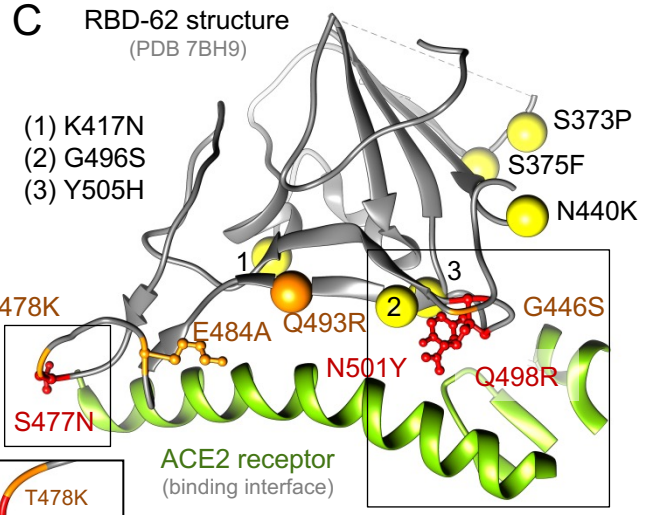

D

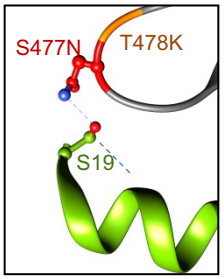

E

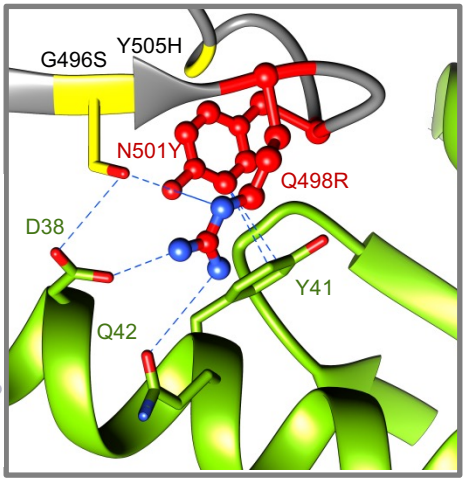

F

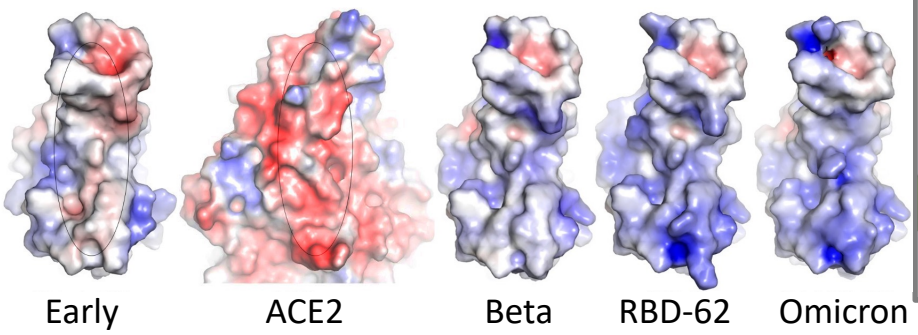

Figure 4

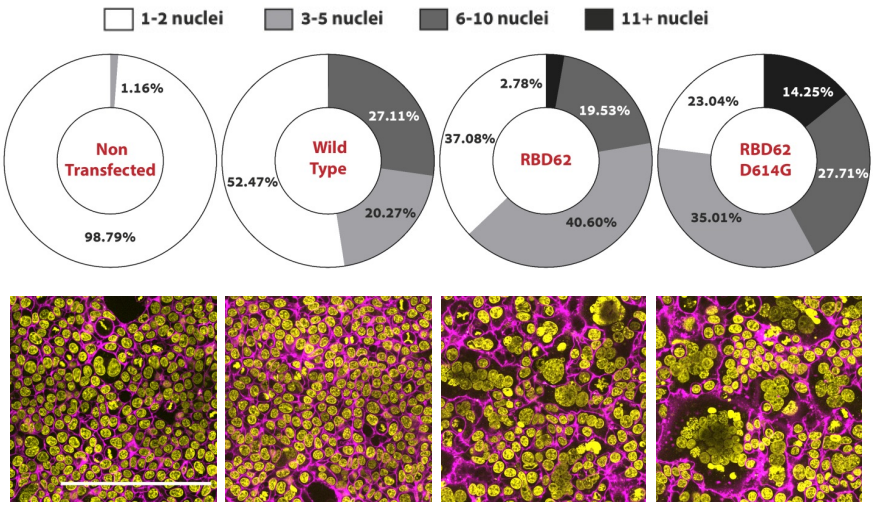
1-2 nuclei
3-5 nuclei
6-10 nuclei
11+ nuclei
Non Transfected
1.16%
98.79%
Wild Type
27.11%
52.47%
20.27%
RBD62
2.78%
19.53%
37.08%
40.60%
RBD62 D614G
23.04%
14.25%
27.71%
35.01%
scale,100 μM

Figure 5

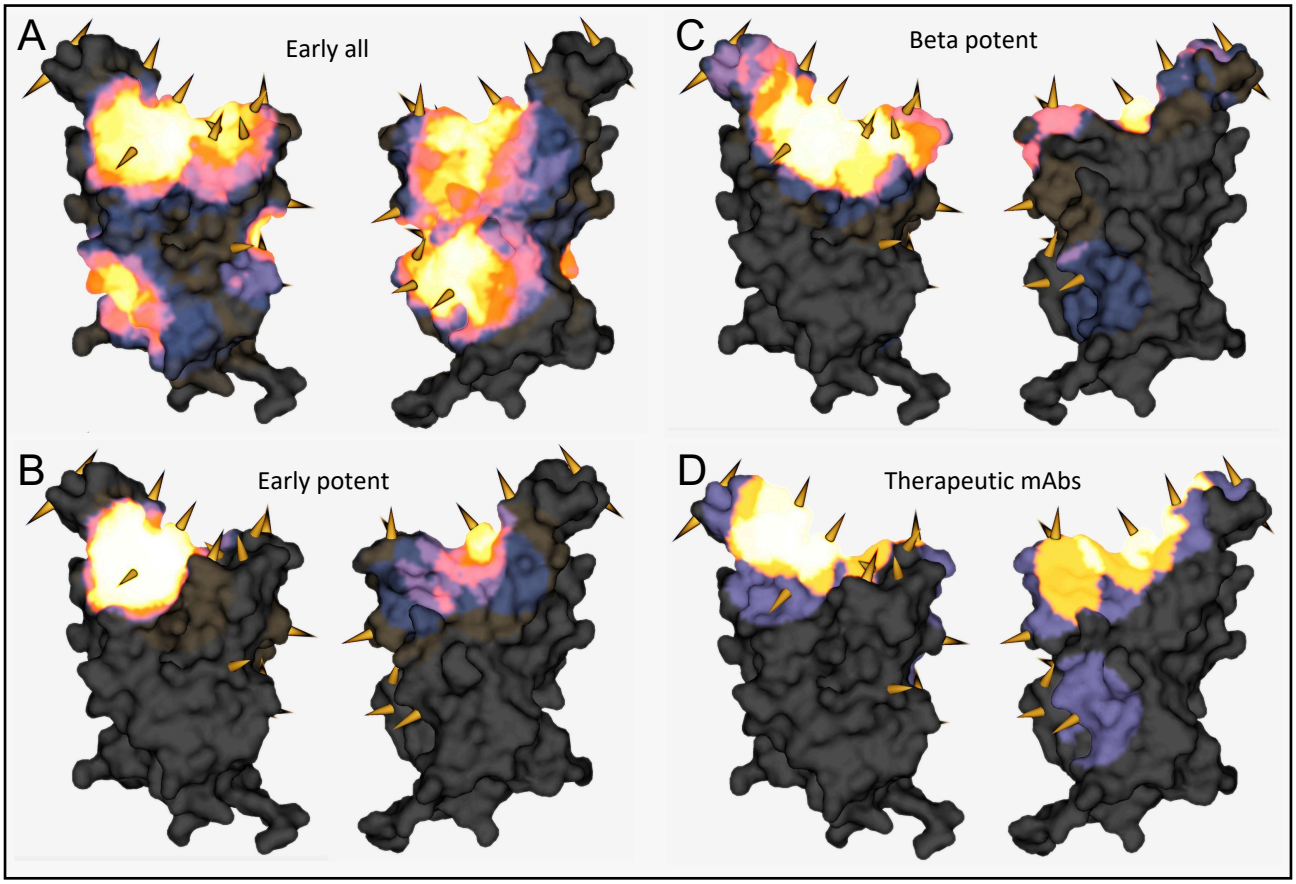

Figure 6

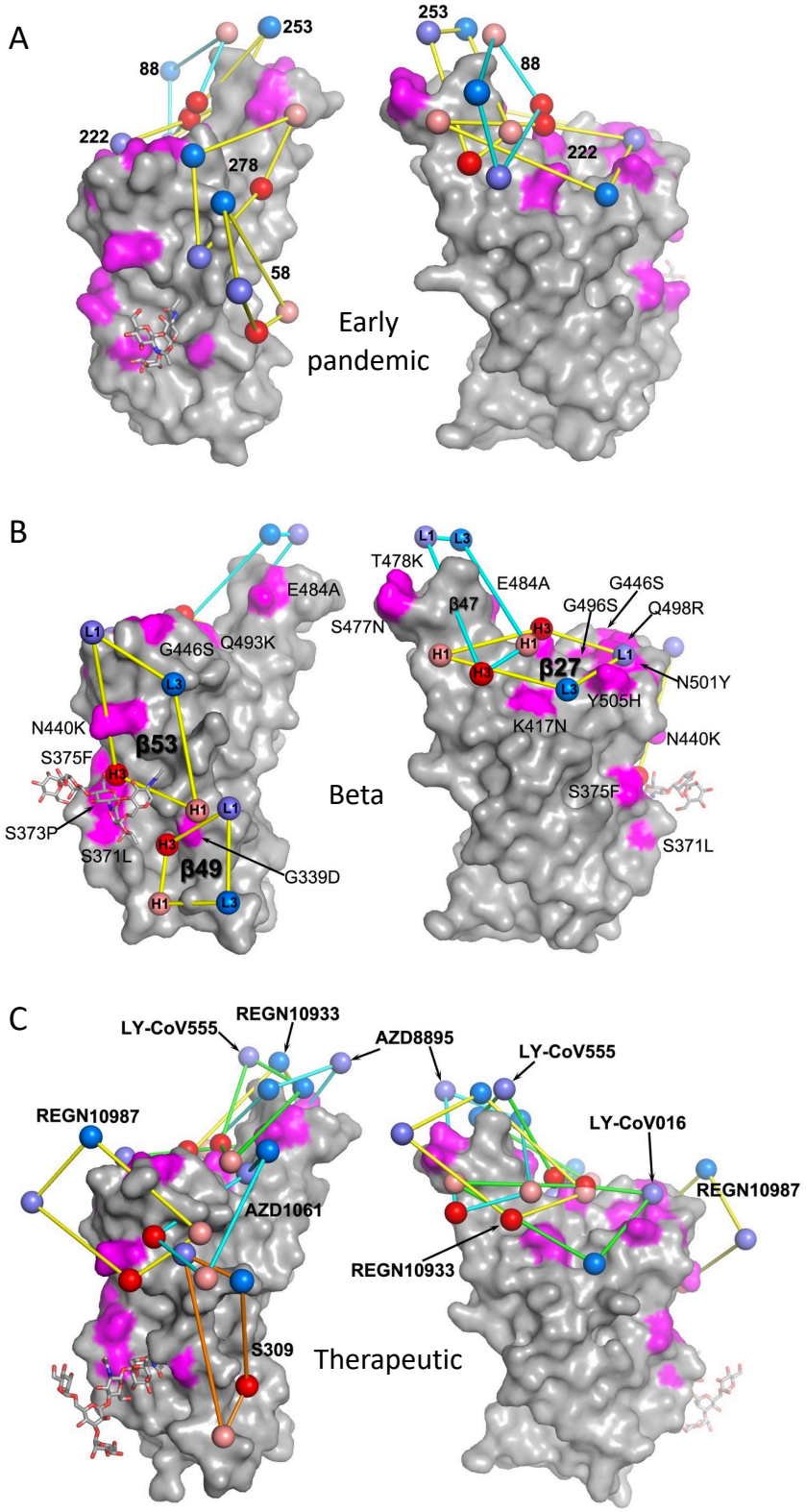
A
253
88
222
278
58
Early
pandemic
253
88
222
B
E484A
L1
G446S
Q493K
L3
N440K
β53
S375F
H3
H1
L1
S373P
S371L
H3
β49
G339D
H1
L3
Beta
L1
L3
T478K
E484A
G446S
β47
G496S
Q498R
S477N
H3
H1
H1
L1
H3
β27
N501Y
L3
Y505H
K417N
N440K
S375F
S371L
C
LY-CoV555
REGN10933
AZD8895
LY-CoV555
REGN10987
LY-CoV016
REGN10987
AZD1061
REGN10933
S309
Therapeutic

Figure 7